Available online at www.sciencedirect.com
SCIENCE DIRECT®
European Journal of Mechanics B/Fluids 24 (2005) 717–732

Forces acting on water droplets falling in oil under the influence of an electric field: numerical predictions versus experimental observations

M. Chiesa [a,*], J.A. Melheim [b], A. Pedersen [b], S. Ingebrigtsen [a], G. Berg [a]

[a] *SINTEF Energy Research, NO-7465 Trondheim, Norway*
[b] *NTNU, NO-7491 Trondheim, Norway*

Received 5 April 2004; received in revised form 17 February 2005; accepted 7 March 2005

Available online 4 May 2005

Abstract

The combination of an electric field and a moderate turbulent flow is a promising technique for separating stable water–oil emulsions. Field-induced charges on the water droplets will cause adjacent droplets to align with the field and attract each other. The present work describes the forces that influence the kinematics of droplets falling in oil when exposed to an electric field. Mathematical models for these forces are presented and discussed with respect to a possible implementation in a multi-droplet Lagrangian framework. The droplet motion is mainly due to buoyancy, drag, film-drainage, and dipole–dipole forces. Attention is paid to internal circulations, non-ideal dipoles, and the effects of surface tension gradients.

Experiments are performed to observe the behavior of a droplet falling onto a stationary one. The droplet is exposed to an electric field parallel to the direction of the droplet motion. The behavior of two falling water droplets exposed to an electric field perpendicular to the direction of their motion is also investigated until droplet coalescence. The droplet motion is recorded with a high-speed CMOS camera. The optical observations are compared with the results from numerical simulations where the governing equations for the droplet motion are solved by the RK45 (Runge Kutta) Fehlberg method with step-size control and low tolerances. Results, using different models, are compared and discussed in detail. A framework is otlined to describe the kinematics of both a falling rigid spherical particle and a fluid droplet under the influence of an electric field.

Keywords: Coalescence; Discrete element method; Electric field; Droplets; Dipole–dipole; Film-thinning

1. Introduction

The oil extracted from offshore reservoirs will normally contain a large and, during the reservoir lifetime, increasing percentage of water in the oil. When the water–oil mixture is passed through the pressure-relief valve, an emulsion with a high percentage of small water drops is formed. Before the oil is pumped on-shore or into tankers, it is desirable to extract the water from this emulsion. Today the separation tanks are mainly built or operated as gravity separators with low flow rates and long residence times, lasting from minutes to tens of minutes. The residence time mainly depends on the sedimentation

* Corresponding author. Post address: NO-7465 Trondheim, Norway.
E-mail address: matteo.chiesa@sintef.no (M. Chiesa).

0997-7546/$ – see front matter
doi:10.1016/j.euromechflu.2005.03.005

Nomenclature

A, A_d	particle surface
a	reduced radius
b	slip length, see Fig. 1
C_d	drag coefficient
$\boldsymbol{d}$	separation vector
$\boldsymbol{E}$, $\boldsymbol{E}_0$	electric field vector
$\boldsymbol{e}_\mathrm{r}$	relative motion vector
$\boldsymbol{F}_\mathrm{e}$	dielectrophoretic force vector
$\boldsymbol{F}_\mathrm{b}$	body force vector
$\boldsymbol{F}_\mathrm{f}$	film thinning force vector
$\boldsymbol{F}_\mathrm{vm}$	virtual mass force
$\boldsymbol{F}_\mathrm{d\text{-}d}$	inter-droplet force vector
$\boldsymbol{F}_\mathrm{d}$	drag force vector
$\boldsymbol{F}_\mathrm{ext}$	external-droplet force vector
$\boldsymbol{F}_\mathrm{fluid}$	fluid-droplet force vector
f^*	correction factor, see Eq. (14)
h	least distance between two particles
i	particle i
r_d	particle radius
r_1	radius of falling particle
r_2	radius of stationary particle
Re_d	particle Reynolds number
$\boldsymbol{u}$	continuous phase velocity vector
$\boldsymbol{v}$	particle velocity vector
$\boldsymbol{v}_i$	velocity vector of particle i
$\boldsymbol{v}_\mathrm{r}$	relative particle velocity vector
V_d	particle volume
$\boldsymbol{x}_\mathrm{i}$	particle position vector
γ_1	magnitude of the surface tension
ϕ	potential function
ε_0	vacuum dielectric constant
ε_d	relative dielectric constant of droplet
ε_oil	relative dielectric constant for oil
θ	angle between $\boldsymbol{E}$ and $\boldsymbol{d}$
λ	viscosity ratio ($\lambda = \mu_\mathrm{d}/\mu_\mathrm{c}$)
μ_d	viscosity of droplet
μ_c	viscosity of the continuous phase
ρ_d	density of the particle phase
ρ_c	density of the continuous phase

velocity of the smallest droplets (e.g. $d < 100$ μm). Electrostatic fields are to some extent used to help smaller drops to coalesce into larger drops that sediment quicker (Eow et al. [1]). The combination of an electric field and a moderate turbulent flow is a promising and compact technique for separating stable water–oil emulsions, see Atten [2]. Charges induced on the water droplets will cause adjacent droplets to align with the field, attract each other and eventually coalesce. The sedimentation velocity increases proportionally to the square of the diameter, and therefore one wishes to get the smallest water droplets to coalesce into larger droplets. The present work describes the forces that influence the kinematics of falling spherical droplets exposed to an electric field. Mathematical models for these forces are presented and discussed with respect to the implementation in a multi-droplet Lagrangian framework. The spherical droplet motion is mainly due to buoyancy, drag, film-drainage, and dipole–dipole forces. General and physically meaningful models for these forces are needed in order to predict the behavior of water–oil emulsion.

In the present work, models for the forces that are believed to determine the motion of droplets falling in oil under the influence of an electric field are reviewed and discussed in detail. A modeling framework that properly accounts for the effect of the different forces on the droplet motion is proposed. Experiments are performed to observe the behavior of a falling droplet exposed to an electrical field and a comparison between observations and predictions is presented in order to assess the performance of the proposed modeling framework. The experiments are designed to isolate the effect of the different forces influencing the kinematics of the droplet.

A first series of experiments is carried out releasing a rigid spherical particle in oil. The released particle has a density and permittivity similar to water. The electric field is parallel to the direction of the particle motion and the velocity of the particle is recorded by a high-speed CMOS camera. The field magnitude is varied.

A second series of experiments is performed releasing water droplets and observing their motion when electric fields of different magnitudes are applied. The effect of internal circulation induced in the droplet becomes important and needs to be taken into account in the proposed modeling framework. The numerical predictions show good agreement when all the effects influencing the droplet kinematics are taken into account.

Further the modeling framework outlined for the single droplet falling towards a stationary one under the influence of an electric field, is applied to predict the kinematics of two water droplets simultaneously released in oil. The electrical field, that is applied perpendicularly to the direction of the motion, induces charges in the water droplets. This causes adjacent droplets to align with the field and to attract each other. The behavior of the two water droplets falling in oil under the influence of an electric field is well predicted by the modeling framework proposed in this work.

2. Theoretical background

The trajectory of a spherical droplet i is calculated by integrating Newton's second law. The law equates the change in momentum per change in time of the droplet with the forces acting on it, and reads:

$$\frac{\mathrm{d}\boldsymbol{x}_i}{\mathrm{d}t} = \boldsymbol{v}_i, \tag{1}$$

$$m_i \frac{\mathrm{d}\boldsymbol{v}_i}{\mathrm{d}t} = \boldsymbol{F}_{\text{fluid}} + \boldsymbol{F}_{\text{ext}} + \boldsymbol{F}_{\text{d-d}}, \tag{2}$$

where m_i, $\boldsymbol{x}_i$, and $\boldsymbol{v}_i$ are the mass, position, and velocity of the droplet. $\boldsymbol{F}_{\text{fluid}}$ represents the vector of forces acting from the fluid on the droplet, $\boldsymbol{F}_{\text{ext}}$ is the external force vector, and $\boldsymbol{F}_{\text{d-d}}$ represents the inter-droplet force vector. Droplet tracking with droplet-droplet interaction has a high computational cost. It is therefore important to keep the computational work necessary to calculate the particle forces as low as possible, since the forces have to be calculated for each particle. Finally, models should be easily implementable in a numerical code.

In the following sections, a modeling framework that properly accounts for the effect of the different forces on the droplet motion is proposed. The electric force between the particle and the droplet is modeled with either the analytical expression obtained by Davis [3], the DID model of Siu et al. [4] or the point-dipole model, see for instance Klingenberg et al. [5]. When describing the motion of a falling water droplet, we have to take into account the effect of internal circulation induced in the droplet. Internal circulation reduces the viscous part of the drag force and therefore the drag coefficient needs to be corrected in order to account for this reduction, as outlined by Happel and Brenner [6]. Furthermore, the surface tension varies over the droplet surface by the effect of surfactants on the interface and by elongation of the droplet, caused by the electric field. This leads to interfacial stresses that inhibit the creation of internal circulation. LeVan [7] suggested how to take into account the effect of surface tension gradient in a numerical framework. Barnocky and Davis [8] showed that the drainage between fluid spheres with arbitrary viscosity is different from rigid particles. The model proposed by Vinogradova [9] is shown in the present work to be useful in order to model the film-thinning between droplets with almost immobile surfaces.

3. Modeling the fluid-droplet and body forces

Fluid droplet forces are transferred from the fluid to the droplets through friction and pressure difference. These forces are expressed by the following surface integral:

$$\boldsymbol{F}_{\text{fluid}} = \int_{\mathcal{A}_\text{d}} (-p_\text{s}\boldsymbol{n}_\text{d} + \boldsymbol{\tau}_\text{d} \cdot \boldsymbol{n}_\text{d})\,\mathrm{d}A \tag{3}$$

where p_s is the pressure at the droplet surface, $\boldsymbol{n}_\text{d}$ represents the unit outward-pointing normal vector and $\boldsymbol{\tau}_\text{d}$ is the shear stress tensor at the droplet surface. The pressure and the tension on the interface are unknown and Eq. (3) has to be modeled. In the Lagrangian framework, the models for the surface integral attempt to provide particular physical meanings. In this work, the fluid droplet force $\boldsymbol{F}_{\text{fluid}}$ is modeled by summing up the drag force $\boldsymbol{F}_\text{d}$, the virtual mass force $\boldsymbol{F}_{\text{vm}}$, and the buoyancy or external body force $\boldsymbol{F}_\text{b}$.

3.1. Drag force

The "steady-state" drag force acts on a droplet in a uniform pressure field when there is no acceleration of the relative velocity between the droplet and the conveying fluid. The force reads:

$$\boldsymbol{F}_\text{d} = \frac{1}{2}\rho_\text{c} C_\text{d} A \|\boldsymbol{u} - \boldsymbol{v}\|(\boldsymbol{u} - \boldsymbol{v}). \tag{4}$$

For a droplet Reynolds number Re_d below 1, the drag coefficient C_d for a rigid sphere is given by:

$$C_\text{d} = \frac{24}{Re_\text{d}}. \tag{5}$$

An internal circulation is induced in fluid spheres, that reduces the viscous part of the drag. For spherical clean bubbles and droplets, the induced internal circulation is accounted for by the Hadamard–Rybczynski formula [10]:

$$C_\text{d} = \frac{24}{Re_\text{d}} \frac{\lambda + 2/3}{\lambda + 1} \tag{6}$$

where $\lambda = \mu_d/\mu_c$ is the viscosity ratio. Surfactants on the interface and elongation of the droplet, caused by the electric field, give a variation in the surface tension. The surface tension gradient leads to interfacial stresses that inhibit the creation of internal circulation. The surface tension gradient is included in the formula by LeVan [7]:

$$C_d = \frac{24}{Re_d} \frac{3\lambda + 2 + 2\kappa(\mu_c r_d)^{-1} + 2/3\gamma_1(\mu_c \|\boldsymbol{u} - \boldsymbol{v}\|)^{-1}}{3\lambda + 3 + 2\kappa(\mu_c r_d)^{-1}}, \tag{7}$$

where also the surface dilational viscosity κ is taken into account. However, in the present work surface dilational viscosity is neglected, $\kappa = 0$. In Eq. (7) it is assumed that the interfacial tension varies as follows:

$$\gamma = \gamma_0 + \gamma_1 \cos\psi \tag{8}$$

where the angle ψ is measured from the front stagnation point.

3.2. Virtual mass force

The virtual mass force $\boldsymbol{F}_{vm}$ is an unsteady force that describes the acceleration of fluid when a particle and the fluid have a relative acceleration. It reads:

$$\boldsymbol{F}_{vm} = \frac{\rho_c V_d}{2}\left(\frac{D\boldsymbol{u}}{Dt} - \frac{d\boldsymbol{v}}{dt}\right). \tag{9}$$

3.3. External body forces

We assume that the droplets have no net charge, hence the electric field as a far-field force can be neglected. On the other hand, the electric field gives rise to induced dipole–dipole interactions between the droplets, which are modeled as inter-droplet forces. Then the gravity is the only external force and the buoyancy force is given by:

$$\boldsymbol{F}_b = (\rho_d - \rho_c) g V_d \boldsymbol{e}_g \tag{10}$$

where g and $\boldsymbol{e}_g$ are the modulus and the direction of the gravity.

3.4. Observations

In the present work, the effects of the pressure gradient, the Basset history force and the lift forces have been neglected. The pressure difference over a small droplet is negligible due to the size of the droplets. The contribution from the gravity is handled separately. Lift forces are due to droplet rotation and shear forces, and can therefore be neglected when a rigid sphere or droplet is falling in a stagnant fluid. Due to the small size of the spheres and the high viscosity of the oil, the particle time scale is very small. Thereby follows that the Stokes number is small and the Basset history force can therefore be neglected, as stated by Michaelides [11].

4. Modeling droplet-droplet forces

The inter-droplet forces are the film thinning forces, due to the drainage of the fluid between the droplets, and the electric forces due to polarization of the conductive water droplets.

4.1. Film-thinning force

The film-thinning force is caused by drainage of the liquid film between two approaching droplets. The derivation of the formulas usually requires that the gap between the particles is small, $h \ll a$, and that the flow is within Stokes regime $Re_d h \ll a$. Here, $a = (r_1 r_2)/(r_1 + r_2)$ is the reduced radius. For rigid spheres the film-thinning force is written as (Davis et al. [12]):

$$\boldsymbol{F}_f = -\frac{6\pi\mu_c a^2 (\boldsymbol{v}_r \cdot \boldsymbol{e}_r)}{h} \boldsymbol{e}_r \tag{11}$$

$\boldsymbol{v}_r$ is their relative velocity vector, and $\boldsymbol{e}_r$ indicates the direction of the relative motion. The size of the droplets is rather small and the electric field elongates the droplets. The elongation builds up a surface-tension gradient that inhibits internal circulation in the droplets. Therefore, the droplet surface is assumed to be immobile. However, when the gap between the droplets approaches zero, the shear stresses between the oil film and the water droplet increase rapidly, and the surface of the droplet starts to move.

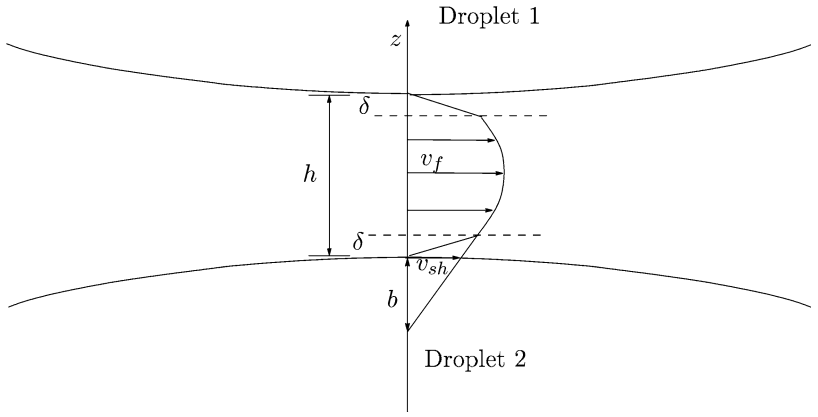

Fig. 1. Illustration of the slip length b near a hydrophobic surfaces. The slip length b is defined as the length characterizing the amount of slippage. δ represents the thickness of the 'slip-layer' and z is the axis between the centres of the droplets.

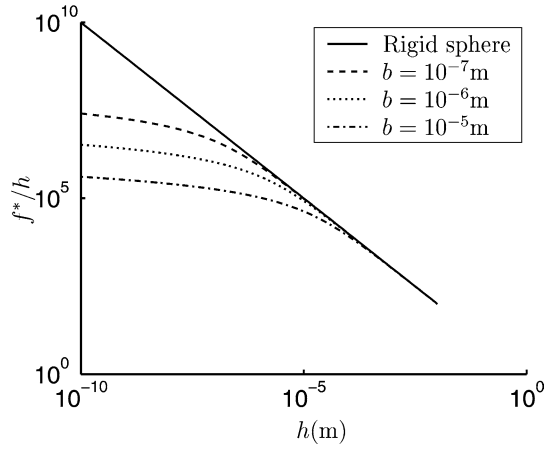

Fig. 2. f^*/h versus h for different values of b compared with the rigid sphere model, Eq. (11).

Such a behavior at large shear stresses is analogous to the slip near hydrophobic and chemically modified surfaces [9,13]. We therefore assume that since the surface is almost immobile, the surface can be thought of as a hydrophobic surface.

The amount of slippage for hydrophobic surfaces is given by the length b see Fig. 1. The slip length b is defined by the slip velocity v_{sh} and the velocity gradient at slip in the following way:

$$v_{\mathrm{sh}} = b\frac{\partial v_{\mathrm{f}}}{\partial z}\bigg|_{z=\delta}. \tag{12}$$

A correction to the rigid particle model, that was proposed by Vinogradova [9] for hydrophobic surfaces, is adopted. The formula of Vinogradova reads

$$\boldsymbol{F}_{\mathrm{f}} = -\frac{6\pi\mu_{\mathrm{c}}a^2(\boldsymbol{v}_{\mathrm{r}}\cdot\boldsymbol{e}_{\mathrm{r}})}{h}f^*\boldsymbol{e}_{\mathrm{r}}, \tag{13}$$

where the correction factor f^* is determined by:

$$f^* = \frac{2h}{6b}\left[\left(1+\frac{h}{6b}\right)\ln\left(1+\frac{6b}{h}\right)-1\right]. \tag{14}$$

Fig. 2 shows f^*/h when h approaches zero for different values of b, compared with the rigid sphere model ($f^* = 1$). For large inter-droplet distances there is no difference between the rigid sphere model and the model of Vinogradova. However, the singularity in the rigid sphere formula when the gap h approaches zero is avoided in the model of Vinogradova; f^*/h approaches a fixed value asymptotically when h approaches zero. This makes the formula of Vinogradova, Eq. (13), attractive from a numerical point of view. In the present work, the value of b is chosen with respect to the droplet size.

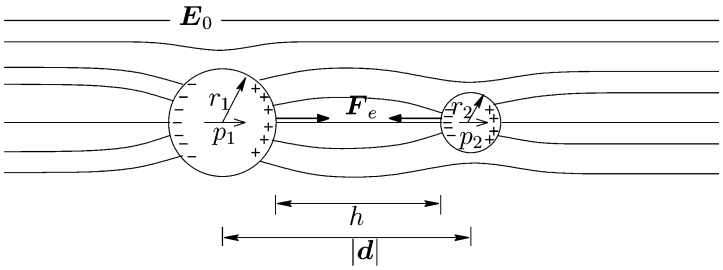

Fig. 3. Electric forces between two conductive spheres.

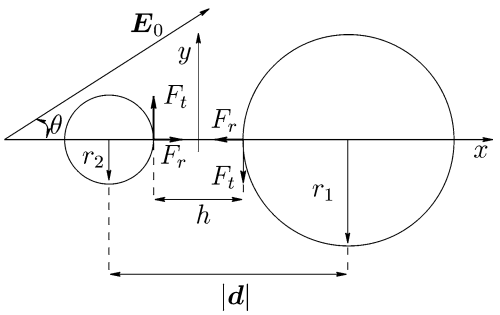

Fig. 4. Radial and tangential force components between two conductive spheres.

Barnocky and Davis [8] studied the drainage between fluid spheres with arbitrary viscosity, from bubbles to rigid particles. The influence of surfactant and the surface tension gradient were not paid any attention. In our case, the droplet at rest is covered with surfactant and is therefore handled as a rigid sphere. The film force formula of Barnocky and Davis [8] for a fluid sphere approaching a rigid sphere reads:

$$\boldsymbol{F}_\mathrm{f} = -\frac{6\pi\mu_\mathrm{c} a^2(\boldsymbol{v}_\mathrm{r}\cdot\boldsymbol{e}_\mathrm{r})}{h}\,\frac{1+0.47\xi+0.0047\xi^2}{1+1.13\xi+0.19\xi^2}\,\boldsymbol{e}_\mathrm{r}, \tag{15}$$

where $\xi = \lambda^{-1}\sqrt{(a/h)}$.

4.2. Electric forces acting on the spherical droplets

Consider an uncharged spherical droplet placed in an insulating medium. The droplet is furthermore subjected to an electric field $\boldsymbol{E}_0$. The field outside a dielectric sphere of permittivity ε_d corresponds to the electric field of a dipole located at the sphere center. The value of this dipole moment $\boldsymbol{p}$ depends on the sphere size, permittivity and the strength of the electric field. Due to the polarization of the droplet, there will be a surface charge distribution preserving zero net charge. In a homogeneous field, the net force on the droplet is zero. Subjected to an inhomogeneous field, the droplet will experience a stronger field at one side than at the other, resulting in a net force acting on the droplet in the direction of the field gradient, a phenomenon called dielectrophoresis. The resulting force is given by $\boldsymbol{F} = (\boldsymbol{p}\cdot\nabla)\boldsymbol{E}$. If the permittivity of the droplet ε_d is higher than the permittivity of the surrounding medium ε_oil, the droplet will move towards the high field region. An inhomogeneous electric field may for instance be set up by a nearby point charge or another dielectric droplet, see Fig. 3. In the latter case, the electrostatic force attracts the two droplets, given that $\varepsilon_\mathrm{d} > \varepsilon_\mathrm{oil}$.

(a) Point-dipole model. For large droplet distances $|\boldsymbol{d}|/r_\mathrm{d} \gg 1$ we can approximate the electrostatic interaction between two droplets as the force between two dipoles located at the sphere centers, see Fig. 3. This is frequently referred to as the *point-dipole* approximation. The forces in the radial direction F_r and in the tangential direction F_t depicted in Fig. 4 is given by (see for instance Klingenberg et al. [5]):

$$F_\mathrm{r} = \frac{12\pi\beta^2\varepsilon_\mathrm{oil}|\boldsymbol{E}_0|^2 r_2^3 r_1^3}{|\boldsymbol{d}|^4}(3\cos^2\theta - 1), \tag{16}$$

$$F_\mathrm{t} = -\frac{12\pi\beta^2\varepsilon_\mathrm{oil}|\boldsymbol{E}_0|^2 r_2^3 r_1^3}{|\boldsymbol{d}|^4}\sin(2\theta), \tag{17}$$

where θ is the angle between the direction of the electrical field $\boldsymbol{E}_0$ and the relative droplet position vector $\boldsymbol{d}$. β is defined as:

$$\beta = \frac{\varepsilon_{\mathrm{d}} - \varepsilon_{\mathrm{oil}}}{\varepsilon_{\mathrm{d}} + 2\varepsilon_{\mathrm{oil}}}. \tag{18}$$

(b) The Dipole-induced-dipole model (DID). The above point-dipole model is not valid when the droplets are approaching each other. In the literature there are different approaches to find the dipole–dipole forces beyond the point-dipole approximation for multiple particles of arbitrary size and position. Clercx and Bossis [14] presented a multi-pole expansion method that gives good results, but the calculation is complex. A more promising method, the *multiple image method*, was presented by Yu et al. [15]. The two first terms in the multiple image method gives the dipole-induced-dipole model (DID) [4], which is simple and numerically efficient. Siu et al. [4] show that the DID model is in good agreement with the experimental values obtained by Klingenberg et al. [5] for $h/r_1 > 0.1$ for equally sized conductive particles. It is customary to write the dipole forces on the form:

$$F_r = \frac{12\pi\beta^2\varepsilon_{\mathrm{oil}}|\boldsymbol{E}_0|^2 r_2^3 r_1^3}{|\boldsymbol{d}|^4}(3K_1\cos^2\theta - 1), \tag{19}$$

$$F_t = -\frac{12\pi\beta^2\varepsilon_{\mathrm{oil}}|\boldsymbol{E}_0|^2 r_2^3 r_1^3}{|\boldsymbol{d}|^4} K_2 \sin(2\theta). \tag{20}$$

For the DID model the coefficients K_1 and K_2, are written as:

$$K_1 = 1 + \frac{\beta r_1^3|\boldsymbol{d}|^5}{(|\boldsymbol{d}|^2 - r_2^2)^4} + \frac{\beta r_2^3|\boldsymbol{d}|^5}{(|\boldsymbol{d}|^2 - r_1^2)^4} + \frac{3\beta^2 r_1^3 r_2^3(3|\boldsymbol{d}|^2 - r_1^2 - r_2^2)}{(|\boldsymbol{d}|^2 - r_1^2 - r_2^2)^4}, \tag{21}$$

$$K_2 = 1 + \frac{\beta r_1^3|\boldsymbol{d}|^3}{2(|\boldsymbol{d}|^2 - r_2^2)^3} + \frac{\beta r_2^3|\boldsymbol{d}|^3}{2(|\boldsymbol{d}|^2 - r_1^2)^3} + \frac{3\beta^2 r_1^3 r_2^3}{(|\boldsymbol{d}|^2 - r_1^2 - r_2^2)^3}. \tag{22}$$

In the limit $|\boldsymbol{d}| \to \infty$ the coefficients K_1 and K_2 approach unity and we recover the point-dipole model given by Eq. (16) and (17).

(c) The analytical solution. Davis [3] derived the potential function ϕ of two conducting spheres by solving Laplace's equation in bi-spherical coordinates with the following constraints:

- At a large distance from the spheres, the potential functions correspond to the background field.
- The spheres are equipotential surfaces and carry an arbitrary net charge.

The forces between two conducting spheres is found by integrating the electrostatic pressure over the sphere surfaces (Maxwell's stress tensor). The solution for uncharged spheres is given by:

$$F_r = 4\pi\varepsilon_{\mathrm{oil}}|\boldsymbol{E}_0|^2 r_2^2(F_1\cos^2\theta + F_2\sin^2\theta), \tag{23}$$

$$F_t = 4\pi\varepsilon_{\mathrm{oil}}|\boldsymbol{E}_0|^2 r_2^2 F_3 \sin(2\theta), \tag{24}$$

where the parameters F_1, F_2, and F_3 are complicated series depending on the ratios $|\boldsymbol{d}|/r_2$ and r_1/r_2. Unfortunately, the computational cost required for calculating F_1 to F_3 is high in a multi-droplet situation. However, this solution is excellent for benchmarking other models in cases with two particles/droplets. For large drop separations $h/r_1 \gg 1$, the force components F_1, F_2 and F_3 approach the values of the point-dipole, Eq. (16) and (17). For small separations $h/r_1 < 1$, F_2 and F_3 takes constant values while F_1 diverges and takes the asymptotic value:

$$F_1 = \frac{4}{3((1 + r_2/2r_1)^4(r_2/|\boldsymbol{d}|)^{-0.8})} \tag{25}$$

see Atten [2].

5. Experimental setup

5.1. General experimental conditions

Experiments have been designed for visual observation of water droplets in oil under the influence of electric field stress, see Berg et al. [16]. A movable 15 mm electrode-gap arrangement is placed vertically inside a cubic test cell with side lengths 150 mm. The cell is placed in an optical bench to obtain a shadow-graphic representation of the water droplets as

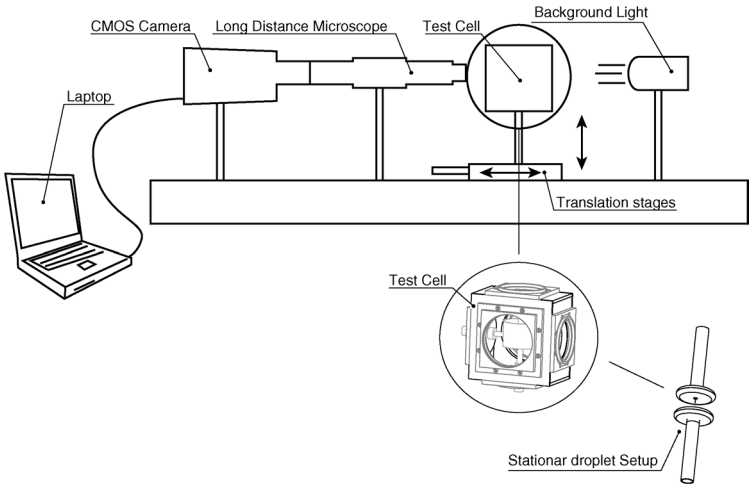

(a)

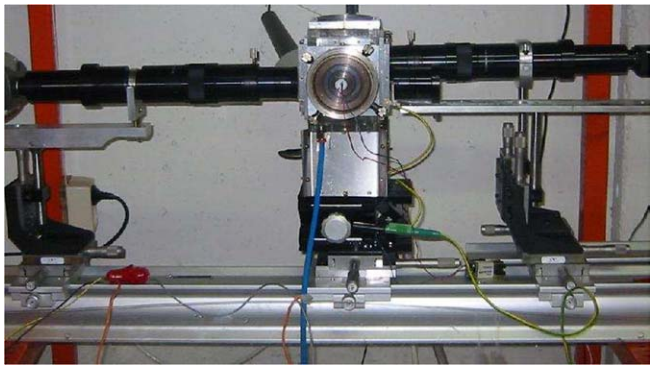

(b)

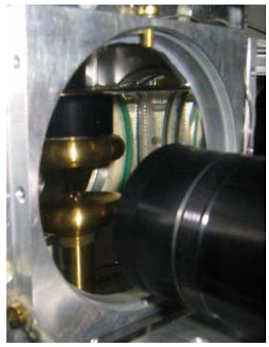

(c)

Fig. 5. Experimental set-up designed for visual observation of the behavior of water droplets in oil, exposed to the effect of an external electric field. (a) Sketch of the experimental set-up, (b) the set-up, (c) the test cell.

shown in Fig. 5. Interactions and coalescence of droplets are recorded with a Phantom V4 high-speed CMOS camera, capable of 1000 frames per second at 512×512 pixels resolution. The position and the velocity of the droplets are digitally extracted from the sequential frames. The uncertainty in measured droplet diameter is less than 5 μm. Distilled water added 3.5 W% of NaCl and Nynäs Nytro 10X oil was used, thus facilitating optical transparency. At 20 °C the oil viscosity is 13.7×10^{-3} Pa s, however some series with rigid spheres were performed at a slightly higher temperature (23–25 °C) and an interpolated viscosity of 12.5×10^{-3} Pa s is used for these simulations. Electric fields are vertical and hence parallel to the droplet-droplet impact vectors.

5.2. Single rigid spherical particle falling in oil

One metal pellet of 4 mm in diameter is positioned at rest and in direct contact with the lower metallic high-voltage electrode. Sub-millimeter sized un-deformable rigid particles are released within the upper ground electrode from a glass capillary. The falling rigid spheres are of Ugelstad type, approximately 150 μm diameter polystyrene base spheres ($\rho = 1050$ kg/m^3) covered with 400 nm silver coating. Glass capillaries are coated with gold to avoid static charge transfer from glass to the particle. Electric fields are applied vertically. They are parallel to the impact vectors and in the range 250–400 V/mm. Bipolar square voltages with frequencies 10 Hz and 100 Hz are used.

5.3. Single water droplet falling in oil

A similar experiment is performed with water droplets. The droplets are released within the upper ground electrode from a glass capillary. Electric fields are vertical to the drop-drop impact vectors and in the range 250–400 V/mm. Bipolar square

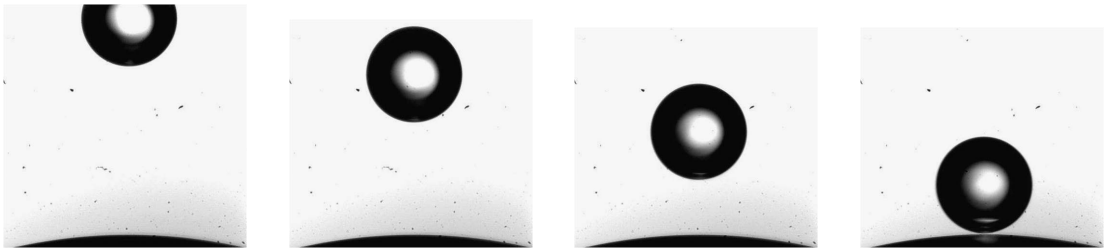

(a) (b) (c) (d)

Fig. 6. Experimental observations of a small water droplet $r_1 = 175$ μm approaching a larger one $r_2 = 2000$ μm at time $t = \sum_i (t_0 + i\Delta t)$ s with $i = 0, 1, 2, 3$. The magnitude of the electric field is $|\boldsymbol{E}_0| = 400$ V/mm. (a) $t = t_0$, (b) $t = t_0 + \Delta t$, (c) $t = t_0 + 2\Delta t$, (d) $t = t_0 + 3\Delta t$.

Table 1
Properties of Nytro 10X, water with a small salt content and rigid sphere particle at 20 °C

	Oil	Water	Rigid sphere
Density ρ	875 kg/m^3	1022 kg/m^3	1206–1210 kg/m^3
Viscosity μ	13.7×10^{-3} Pa s	0.98×10^{-3} Pa s	∞
Relative permittivity ε	2.2	1000	1000

Table 2
Experimental series

Electric field (V/mm)	Rigid sphere radius (μm)	Droplet radius (μm)
0	82.5	
250	70.5	105
300	70.5	110 and 58
400	72	110

voltages with frequencies 10 Hz and 100 Hz are used. The glass capillaries are made hydrophobic to ease the release of generated droplets, and coated with gold to avoid static charge transfer from glass to water. Fig. 6 shows a typical collision between a 350 μm diameter falling water droplet and a 4 mm diameter stationary drop. Fig. 6(d) is the picture taken before the coalescence takes place. The gap between the droplets in this case is approximately $h = 20$ μm. Such a gap is dependent on the magnitude of the electric field, but anyway it gives a physical indication of how to interpret the slip length b in the model of Vinogradova for the film-thinning force, Eq. (13). The graphs in Fig. 2 show only minor differences between the rigid sphere model and the model of Vinogradova for $h > 20$ μm when $b \geqslant 1$ μm. This means that the correction for almost immobile surfaces, Eq. (14), has neglictable influence on the results for gaps $h >$ μm. For smaller gaps $h <$ μm the uncertainties regarding the position of the droplet surface is large, in particular for high electric fields.

5.4. Two water droplets falling in oil

Two sub-millimeter-sized water droplets are released within the upper ground electrode from a glass capillary as previously explained. The two water droplets fall freely in Nytro 10X oil (see Table 1) and after $t = 0.56$ sec an electric 50 Hz field of magnitude 280 V/mm is applied. The electric field is perpendicular to the direction of the droplets motion. A sinusoidal voltage with frequency 50 Hz is used. Droplet interactions and coalescence are recorded with the CMOS camera.

6. Results and discussion

6.1. Numerical set-up

Numerically, the governing equations (1) and (2) are solved with a Runge–Kutta Fehlberg 4-5 solver with step-size control, see for instance Hairer et al. [17]. Accurate solution of the equation system is ensured by using a relative tolerance of 10^{-5} and an absolute tolerance of 10^{-25}. The expression for the forces described in Section 3 are used. An ideal bipolar squared voltage is assumed.

6.2. Single rigid spherical particle falling in oil

Fig. 7 shows a comparison between experimental observations and numerical predictions of the kinematics of a rigid spherical particle falling towards an electrode. No electric field is applied. The b constant in the expression of Vinogradova equation (13) used in the numerical calculation is 10^{-7} m. The velocity of the rigid sphere is plotted versus the normalized distance h/r_1. The good agreement between observations and predictions shows that drag equation (4), buoyancy equation (10) and film-drainage equation (13) are well modeled in our numerical framework.

A comparison between observed and predicted velocities versus normalized particle-surface distance h/r_1 for rigid spheres under the influence of an electric field is plotted in Fig. 8. The buoyancy, drag and film-drainage are modeled as in the previous numerical exercise presented in Fig. 7. Fig. 8(a) shows the effect of different electric field magnitudes on the falling velocity of the particle. The analytical model by Davis, Eq. (23) and (24), is used in the numerical calculations of the particle velocity. A good agreement between numerical results and experimental observations is obtained. The velocity of the falling droplet observed when the magnitude of the electric field is greatest, $|\boldsymbol{E}_0| = 400$ V/mm, is higher than for weaker field magnitudes. This follows expectations. Fig. 8(b) shows a comparison between observed and predicted velocities obtained using different models for the induced electrical forces. The magnitude of the applied electric field is $|\boldsymbol{E}_0| = 300$ V/mm. The point dipole model does not provide satisfactory results. The accuracy of the results obtained by using the DID model is high as long as the droplets are not too close to each other. Therefore, due to its applicability to a multi-droplet system, the DID model is believed to be the best candidate to model a water-in-oil emulsion.

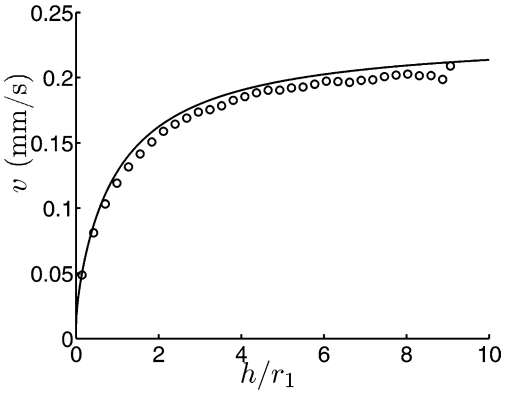

Fig. 7. Predicted and observed velocity versus normalized particle surface distance for a falling rigid sphere with radius $r_d = 82.5$ μm. No electric field is applied.

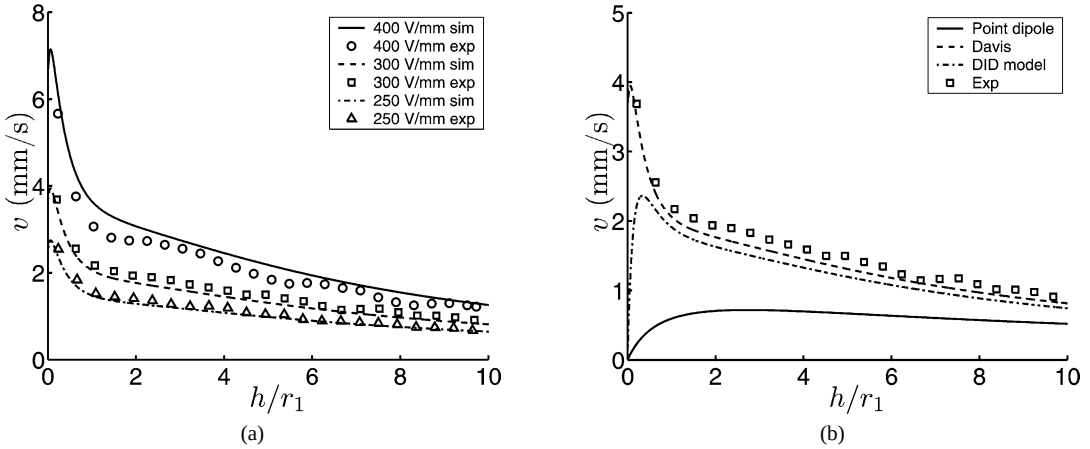

Fig. 8. Observed and predicted velocities versus normalized particle surface distance h/r_1 for rigid spheres. The radius of the sphere is $r_1 \approx 70$ μm and the slip length in Eq. (13) is $b = 10^{-7}$ m.

6.3. Single water droplet falling in oil

When comparing predictions and the observations of the motion of a falling fluid droplet, we have to take into account the effect of internal circulation induced in the droplet. Internal circulation reduces the viscous part of the drag force and therefore the drag coefficient needs to be corrected, as outlined in Section 3.1. Furthermore, the surface tension of the droplet is varied by the effect of surfactants on the interface and by elongation of the droplet, caused by the electric field. This leads to interfacial stresses that inhibit the creation of internal circulation. LeVan [7] suggested how to take into account the effect of surface tension gradients in a numerical framework. Barnocky and Davis [8] derived expressions for the drainage between fluid spheres with arbitrary viscosity. The model proposed by Vinogradova [9] takes interfacial slip effects into account. Although Vinogradova [9] proposed a correction for hydrophobic surfaces, the present work shows that Eq. (13) and (14) can be used with good results for almost stationary surfaces as well. A comparison between observed and predicted velocities versus normalized particle surface distance h/r_1 for fluid droplets under the influence of an electric field is plotted in Fig. 9. The average radius of the droplets is $r_1 \approx 110$ μm. The slip length in the Vinogradova equation (13) is $b = 10^{-6}$ m and the magnitude of the interfacial tension gradient in Eq. (6) is $\gamma_1 = 10^{-5}$ N/m.

Fig. 9(a) shows the effect of different electric field magnitudes on the falling droplet velocity. The analytical model by Davis, Eq. (23) and (24), is used in the numerical calculations of the particle velocity and a good agreement between numerical results and experimental observations is obtained. Fig. 9(b) shows a comparison between observed and predicted velocities obtained using different models for the induced electrical forces. The magnitude of the applied electric field is $|\boldsymbol{E}_0| = 300$ V/mm. The

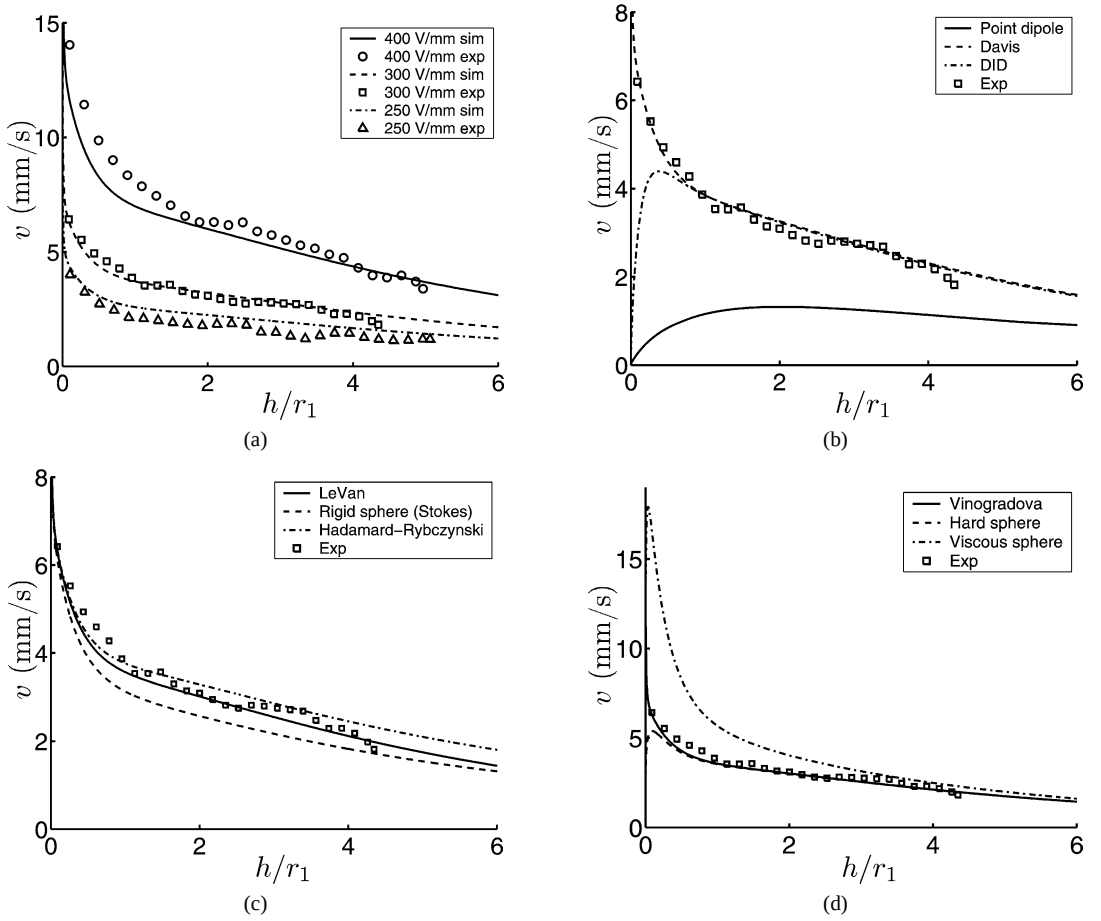

Fig. 9. Observed and predicted velocities versus normalized droplet surface distance h/r_1 for water droplets. The radii of the droplets are $r_1 \approx 110$ μm. The slip distance in Eq. (13) is $b = 10^{-6}$ m and the magnitude of the interfacial tension gradient in Eq. (6) is $\gamma_1 = 10^{-5}$ N/m. (a) The Davis expressions are used in the numerical calculations. (b) Different models for the induced electrical forces are compared, $|\boldsymbol{E}_0| = 300$ V/mm. (c) Different drag force models are compared, $|\boldsymbol{E}_0| = 300$ V/mm. (d) Different drainage models are compared, $|\boldsymbol{E}_0| = 300$ V/mm.

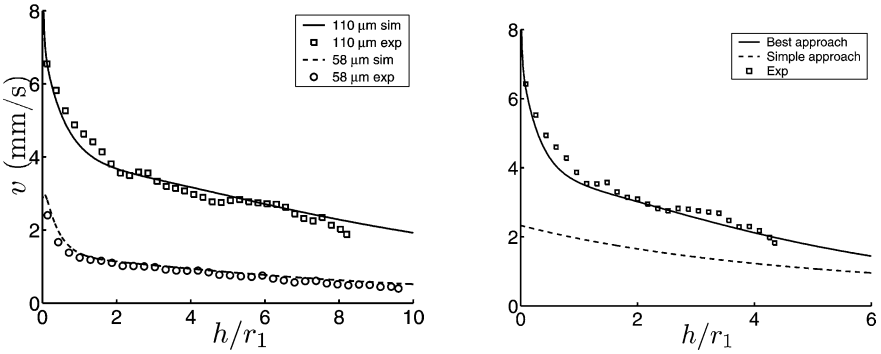

Fig. 10. Observed and predicted velocities versus normalized droplet surface distance h/r_1 for water droplets. (a) Different droplet size $r_{\text{big}} = 110$ μm, $r_{\text{small}} = 58$ μm. $|\boldsymbol{E}_0| = 300$ V/mm. The slip distance in the Vinogradova model is $b = 10^{-6}$ m for r_{big} and $b = 10^{-7}$ m for r_{small}. Furthermore $\gamma_1 = 10^{-5}$ N/m for r_{big} and $\gamma_1 = 2 \times 10^{-5}$ N/m for r_{small}. (b) 'Simple' versus 'best' modeling at $|\boldsymbol{E}_0| = 300$ V/mm. Droplet size $r = 110$ μm. The simple modeling strategy includes: point dipole, rigid sphere drag and no film force. The best modeling strategy employs the models of Davis, LeVan, and Vinogradova.

same trend as previously observed for the rigid spheres is observed. Fig. 9(c) shows the results obtained by different drag force models. The electric field is constant $|\boldsymbol{E}_0| = 300$ V/mm. The Davis analytical expressions, the Vinogradova model with $b = 10^{-6}$ m and Eq. (7) with $\gamma_1 = 10^{-5}$ N/m are used in the calculations. The best agreement is obtained when the equation proposed by LeVan equation (7) is used in the numerical calculations.

Fig. 9(d) shows the results obtained for different drainage models. The electric field is kept constant, $|\boldsymbol{E}_0| = 300$ V/mm. The Davis analytical expressions and the LeVan drag force model are used in the calculations. In the formula of Vinogradova, $b = 10^{-6}$ m. The best agreement is obtained when the model proposed by Vinogradova equation (13) is used. The viscous sphere model equation (15), gives a severe overestimation of the velocity, and shows that the surface cannot be handled as ideal. The results obtained from the hard-sphere model seem to agree well with the experimental observations expect when the droplets are very close.

Fig. 10 shows a comparison between observed and predicted velocities versus normalized droplet surface distance h/r_1 for water droplets of different radii. In Fig. 10(a), two different droplet sizes $r_{\text{big}} = 110$ μm, $r_{\text{small}} = 58$ μm are considered. The electric field is constant, $|\boldsymbol{E}_0| = 300$ V/mm. The slip distance in the Vinogradova model is $b = 10^{-6}$ m for the biggest droplet and $b = 10^{-7}$ m for the smallest one. Furthermore, the value of γ_1 for the big droplet is $\gamma_1 = 10^{-5}$ N/m and $\gamma_1 = 2 \times 10^{-5}$ N/m for the small one. The numerical predictions agree very well with the experimental observations. In Fig. 10(b), numerical predictions obtained with two different approaches are compared to experimental observations. The "simple approach" adopts point-dipole, rigid-sphere drag and no film-thinning force, while the "best approach" employs the models of Davis, LeVan, Vinogradova. The agreement between predictions and observations obtained by means of the "simple approach" is not satisfactory.

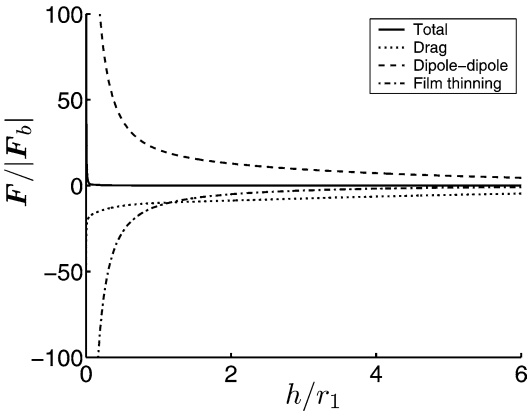

Fig. 11. Contribution of the force components, scaled with the buoyancy force.

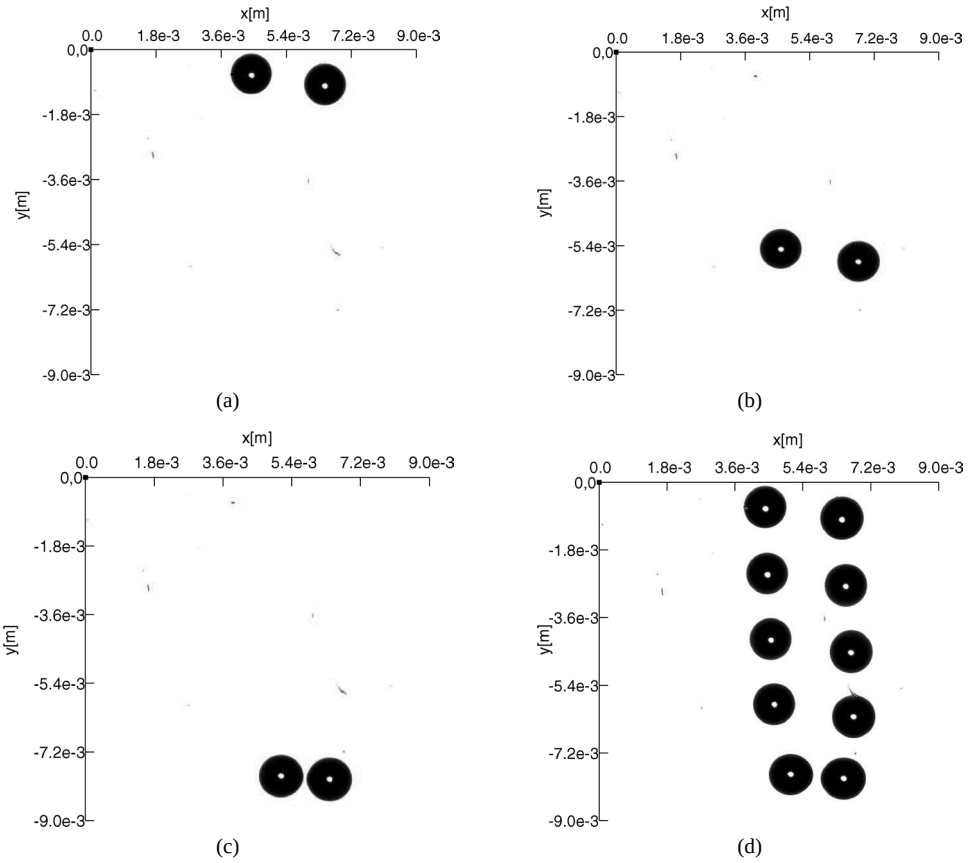

Fig. 12. Experimental observation. Two free falling droplets in oil at time $t = 0.0$ s. (b) At time $t = 0.56$ s an external field perpendicular to the direction of the droplet motion is applied $|\boldsymbol{E}_0| = 280$ V/mm. (c) At time $t = 0.80$ s the droplets are just about to coalesce. (d) Represents a series of picture at different time intervals.

Fig. 11 shows the contribution of the different forces normalized by the buoyancy force for the $|\boldsymbol{E}_0| = 300$ V/mm case. The film-thinning and drag forces almost balance the electric force until the droplets are very close.

6.4. Two water droplets falling in oil

The modeling framework outlined for the single droplet falling towards a stationary one under the influence of an electric field is used in the present work to predict the kinematics of two water droplets simultaneously released in oil. The radius of the smallest droplet placed on the left hand side in the experiments is $r_1 = 533$ μm and the radius of the biggest one is $r_2 = 553$ μm. The uncertainty in the measured droplet diameter is less than 10 μm. The position of the droplets is recorded with a high-speed CMOS camera and it is digitally extracted from the sequential frames [18]. Fig. 12 shows a series of frames at different times. At time $t = 0.0$ s, see Fig. 12(a), the droplets are released in the oil. The droplets fall down because of gravity, and at time $t = 0.56$ s an electric field perpendicular to the direction of the droplets motion is applied. Fig. 12(b) shows the droplets' position at the instant when the field is applied. Fig. 12(c) shows the droplets' position at time $t = 0.80$ s, when the droplets are just about to coalesce. The electrical field induces charges on the water droplets and this causes adjacent droplets to align with the field and attract each other. Fig. 12(d) shows a sequence of frames taken at a time interval $\Delta t = 0.20$ sec where the effect of the electric field on the droplet kinematics is observable. The biggest droplet is observed to fall at a higher speed than the smallest one and therefore the angle between the center of the droplets and the normal to the droplets motion increases. This trends is reversed when a field normal to the droplet motion is applied and the droplets tend to align with the field.

Fig. 13 shows a numerical prediction of the kinematics of the two falling droplets when the Davis model is employed together with the models of LeVan, and Vinogradova, as previously explained. There is a good correspondence between observed and predicted velocities. For this reason, the observed y-coordinates of the two droplets are here compared to the predictions obtained when using different models for the electric forces. Fig. 14 shows a comparison between the predicted and observed

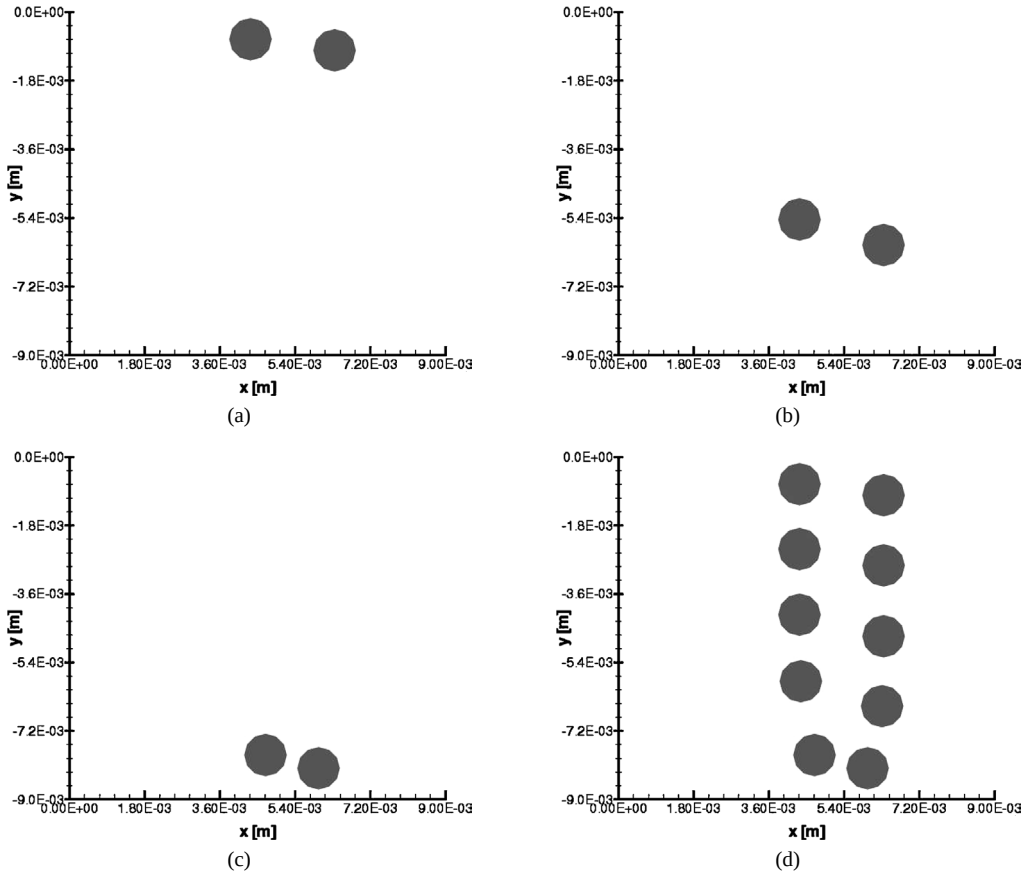

Fig. 13. Numerical prediction of the kinematic of two water droplets falling in a stagnant oil by means of the 'best approach' employing the models of Davis, LeVan, Vinogradova. (a) Two droplets are released at time $t = 0$ s. (b) At time $t = 0.56$ s an external field perpendicular to the direction of the droplet motion is applied $|\boldsymbol{E}_0| = 280$ V/mm. (c) At time $t = 0.80$ s the droplets are just about to coalesce. (d) Represents a series of results at different time intervals.

y-coordinate of the two droplets as a function of time. The Davis, the DID and the point dipole models are used together with the models of LeVan, and Vinogradova to predict the time of coalescence and droplets kinematic of the droplets. The results obtained by the Davis model predict well the time of coalescence and the overall kinematics of the two droplets. The simulation obtained by the other two models overestimated the collision time. This result is coherent to what was presented in Fig. 9.

The point dipole model underestimates the effect of the electric forces on the kinematics of the droplets. In the numerical predictions, the biggest droplet is falling at a higher speed than the smallest one, as observed in the experiment. The predicted fall of the smallest droplet up to time $t = 0.56$ s agrees well with the experimental observations see Fig. 14(a) and (b). On the other hand, the predicted fall of the biggest droplet is slightly overestimated, see Fig. 14(c) and (d). This is most probably due to the uncertainty related to the measured droplets size. There is no reason to believe that the drag model needs to be reviewed in order to account for the vicinity of the other droplet since they fall side by side. The drag force acting on the droplets is affected by the presence of a second droplet in its vicinity when the droplet lies in the boundary layer of the neighboring one.

The predicted and observed normalized distance h/r_1 between the droplet centers as a function of time is plotted in Fig. 14(e). The time to collision predicted by means of the Davis equations agrees well with the coalescence time observed in the experiments. The DID model also provides satisfactory results. The deviation between the Davis and the DID models regarding the time of collision is believed to be insignificant compared to the uncertainties related to the modeling of the coalescence phenomenon. Therefore, due to its applicability to a multi-droplet system, the DID model is believed to be the best candidate to model a water-in-oil emulsion together with the models of LeVan, and Vinogradova.

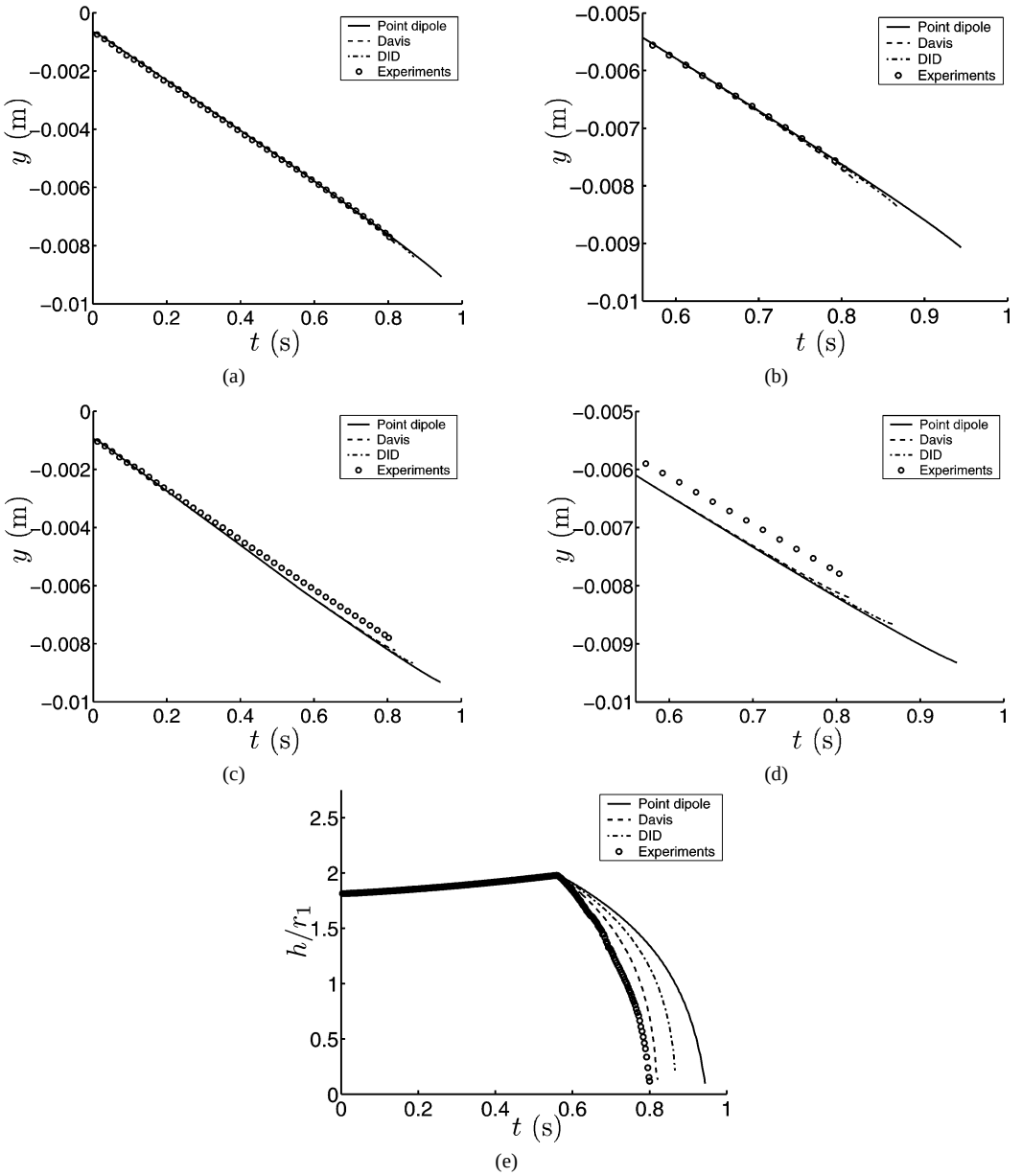

Fig. 14. Observed and predicted vertical coordinate versus time of (a) droplet 1 and (c) of droplet 2. (b) and (c) are close up of what presented in respectively (a) and (c). Observed and predicted normalized distance between the two droplets versus time (e). Different models for the electrical forces are adopted together with the models of LeVan, and Vinogradova.

7. Observations and conclusions

A modeling framework that properly accounts for the effect of the different forces on the droplet motion is proposed. The comparison between observed and predicted velocities versus normalized droplet surface distance, h/r_1, for fluid droplets shows a good agreement when all the effects influencing the droplet kinematics are accounted for.

In the case of rigid particles the models used to describe drag, Eq. (4), buoyancy, Eq. (10) and film-drainage, Eq. (13) give good agreement with the experimental observations. The effect of the electric forces on the motion of the rigid particles is well taken into account when the model of Davis, Eq. (23) and (24), is used in the numerical calculations. It was also observed that the DID model, Eq. (19), provides good results, as long as the normalized droplet surface distance is not too small.

When the motion of fluid droplets is to be predicted, the simple model for drag, buoyancy and film-drainage used for rigid particles is not longer valid. The effect of internal circulation induced in the droplets has to be taken into account, together with the variation of the surface tension of the droplets due to the electric field. In the present work, different models are assessed. The use of the model proposed by LeVan, Eq. (7), for the drag force, by Vinogradova, Eq. (13), for the film-thinning force, and the Davis analytical expression, Eq. (23) and (24), provide numerical predictions that agree well with the experimental observations.

The motion of two fluid droplets simultaneously released in oil has also been predicted. The effect of internal circulation induced in the droplets is taken into account, together with the variation of the surface tension of the droplets due to the electric field. The electric field is applied normally to the motion of the droplets after 0.56 s of free fall. The droplets tend to align with the field before they eventually coalesce with each other. This behavior is well predicted by the model proposed by LeVan for the drag force, by Vinogradova for the film-thinning force and the Davis' analytical expression. The use of different models to take into account the effect of electrical fields is also assessed. The "time of coalescence" predicted by means of the Davis equations agrees well with that observed in the experiments.

The work presented here provides all the elements necessary to model the behavior of water emulsified in oil under the influence of an external electrical field. The kinematics of the water droplets can be predicted by employing the models described in the paper. The DID model, for instance, can be used instead of the Davis model due to its applicability to a multi droplet system. The deviation between Davis and DID model for small inter-droplet distances is believed to be insignificant compared to the uncertainties related to the modeling of coalescence. Furthermore, the correction of the film-thinning forces proposed by Vinogradova eliminates the singularity of the rigid-sphere formula, thus making the Vinogradova model attractive from a numerical point of view. In conclusion, the proposed framework can be utilized to describe the behavior of a water in oil emulsion subjected to an electrical field.

Acknowledgements

The authors are thankful to VetcoAibel, Statoil and the Research Council of Norway for supporting the present work. In particular we are grateful to Lars Lundgaard and Svend Tollak Munkejord for fruitful discussion during the preparation of the manuscript.

References

[1] J.S. Eow, M. Ghadiri, A.O. Sharif, T.J. Williams, Electrostatic enhancement of coalescence of water droplets in oil: a review of current understanding, Chem. Eng. J. 84 (2001) 173–192.
[2] P. Atten, Electrocoalescence of water droplets in an insulating liquid, J. Electrostatics 30 (1993) 259–270.
[3] M.H. Davis, Two charged spherical conductors in a uniform electric field: forces and field strength, Rand. Corp. Memorandum RM-3860-PR, January 1964.
[4] Y.L. Siu, T.K.W. Jones, K.W. Yu, Interparticle force in polydisperse electrorheological fluid: beyond the dipole approximation, Comput. Phys. Commun. 142 (2001) 446–452.
[5] D.J. Klingenberg, F. van Swol, C.F. Zukoski, The small shear rate response of electrorheological suspensions. II Extensions beyond the point-dipole limit, J. Chem. Phys. 94 (9) (1991) 6170–6178.
[6] J. Happel, H. Brenner, Low Reynolds Number Hydrodynamics, Martinus Nijhoff, The Hague, The Netherlands, 1983.
[7] D.M. LeVan, Motion of droplet with a Newtonian interface, J. Colloid Interface Sci. 83 (1) (1981) 11–17.
[8] G. Barnocky, R.H. Davis, The lubrication force between spherical drops, bubbles and rigid particles in a viscous fluid, Int. J. Multiphase Flow 15 (1989) 627–638.
[9] O.I. Vinogradova, Drainage of a thin liquid film confined between hydrophobic surfaces, Langmuir 11 (1995) 2213–2220.
[10] C. Crowe, M. Sommerfeld, Y. Tsuji, Multiphase Flows with Droplets and Particles, second ed., CRC Press, Boca Raton, FL, ISBN 0-8493-9469-4, 1998.
[11] E.E. Michaelides, Hydrodynamic force and heat/mass transfer from particles, bubbles, and drops – the Freeman scholar lecture, J. Fluids Eng. Trans. ASME 125 (2003) 209–238.
[12] R.H. Davis, J.A. Schonberg, J.M. Rallison, The lubrication force between two viscous drops, Phys. Fluids A 1 (1) (1989) 77–81.
[13] Y. Zhu, S. Granick, No-slip boundary conditions switches to partial slip when fluid contains surfactant, Langmuir 18 (2002) 10058–10063.
[14] H.J.H. Clercx, G. Bossis, Many-body electrostatic interactions in electrorheological fluids, Phys. Rev. E 48 (4) (1993) 2721–2737.
[15] K.W. Yu, T.K.W. Jones, Interparticle forces in polydisperse electrorheological fluids, Comput. Phys. Commun. 129 (2000) 177–184.
[16] G. Berg, L. Lundgaard, M. Becidan, S.R. Sigmond, Instability of electrically stressed water drops in oil, ICDL 14th International Conference on Dielectric Liquids.
[17] E. Hairer, S.P. Nørsett, G. Wanner, Solving Ordinary Differential Equations I, second ed., Springer, Berlin, ISBN 3-540-56670-8, 1992.
[18] A. Pedersen, E. Ilstad, A. Nysveen, Forces and movment of water droplets in oil caused by applied electric field, IEEE Conference on Electric Insulation and Dielectric Phenomena, submitted for publication.